Ninth International Conference on
THIN-WALLED STRUCTURES – ICTWS2023
Sydney, Australia, Nov 29 – Dec 1, 2023

# WEB CRIPPLING OF STAINLESS STEEL BUILT-UP I-SECTIONS UNDER END-TWO-FLANGE LOADING

**Yannan Jing*, Ke Jiang**, Yating Liang*** and Ou Zhao***

* School of Civil and Environmental Engineering, Nanyang Technological University, Singapore
e-mails: YANNAN001@e.ntu.edu.sg, ou.zhao@ntu.edu.sg

** Department of Civil and Natural Resources Engineering, University of Canterbury, Christchurch, NZ
e-mail: ke.jiang@canterbury.ac.nz

*** School of Engineering, University of Glasgow, Glasgow, UK
e-mail: Yating.Liang@glasgow.ac.uk

**Keywords**: Stainless Steel; Built-up I-section; End-Two-Flange loading; Numerical modelling; Screw arrangements; Web crippling.

**Abstract**. *This paper presents experimental and numerical investigations into the web crippling behaviour and load-carrying capacities of austenitic and duplex stainless steel built-up I-section members under a concentrated transverse loading condition – End-Two-Flange loading. An experimental programme was conducted on 23 austenitic and duplex stainless steel built-up I-section specimens. Following the experimental programme, a numerical modelling programme was performed, where finite element models were firstly developed to repeat the tests and then used to conduct parametric studies. Based on the test and numerical data, the accuracy of the existing design rules for stainless steel built-up I-section members failing by web crippling, as set out in the European Code and American specification, was assessed. The assessment results indicated that the European Code resulted in overly conservative and scattered failure load predictions, while the American specification led to unconservative and scattered failure load predictions. Therefore, an improved design approach was proposed and shown to provide substantially improved failure load predictions.*

## 1 INTRODUCTION

Stainless steel has emerged as an environmentally friendly construction material in the field of building engineering, owing to its remarkable ductility, corrosion resistance, and recyclability [1, 2]. Under concentrated transverse loading, the stainless steel members are subject to non-uniform distributed stresses and thus localised failure, i.e. web crippling. Hence, in order to study the structural behaviour of stainless steel members failing by web crippling, experimental and numerical investigations have been conducted and briefly reviewed herein. The web crippling behaviour and resistances of cold-formed stainless steel channel section members were experimentally and numerically studied by Yousefi et al. [3, 4], and concluded that the existing design codes provided inaccurate failure load predictions. Zhou and Young [5, 6], Cai and Young [7] and Li and Young [8] conducted a series of experimental and numerical investigations into cold-formed stainless steel square and rectangular hollow sections, and highlighted the inaccuracy of existing design codes. Built-up sections, which are composed of two or more component sections assembled by screws or welds, are ease of fabrication and offer flexibility in cross-section shapes. Therefore, built-up sections are gaining increasing use in the cold-formed steel industry. However, research into stainless steel built-up section members failing by web crippling remains scarce.

This paper focuses on the web crippling behaviour and load-carrying capacities of austenitic and duplex stainless steel built-up I-section members under End-Two-Flange loading. Experiments were firstly conducted on 23 austenitic and duplex stainless steel built-up I-section specimens, with the test results fully reported. A numerical modelling programme was carried out, including a validation study, where finite element models were validated against the test results, and a series of parametric studies, where the validated finite element models were employed to generate further numerical data. All the experimental and numerical data were used to assess the accuracy of the existing codified design rules for stainless steel built-up I-section members failing by web crippling, as prescribed in EN 1993-1-4 [9] and ASCE/SEI 8-22 [10]. Finally, an improved design approach was proposed.

## 2 EXPERIMENTAL PROGRAMME

### 2.1 Test specimens

A total of 23 stainless steel built-up I-section specimens, designed with different cross-section dimensions, screw arrangements and bearing lengths, were adopted in the experimental programme. As shown in Figure 1, each built-up I-section specimen consisted of two identical press-braked stainless steel channel section members, which were connected by self-tapping screws in a back-to-back manner. Grade EN 1.4301 austenitic stainless sheets with nominal thicknesses of 1.0 mm and 2.0 mm and grade EN 1.4462 duplex stainless steel sheets with a nominal thickness of 1.5 mm were employed to fabricate seven built-up I-sections, with nominal cross-section geometries of 100 × 80 × 1.0, 125 × 90 × 1.0, 100 × 80 × 2.0, 125 × 90 × 2.0, 150 × 100 × 2.0, 100 × 80 × 1.5 and 125 × 90 × 1.5 (outer cross-section height $H$ × flange width $B$ × thickness $t$ in mm – see Figure 1). Table 1 reports the measured geometric dimensions of stainless steel built-up I-section specimens, where $H$ is the outer cross-section height, $B$ is the flange width, $t$ is the thickness, $r_i$ is the inner corner radius of the component channel sections, $L$ is the member length, $N$ is the bearing length and $e$ is the distance from the centre of the screw to the outer face of the nearest flange. There are three types of screw arrangements for each built-up I-section, including two rows of screws with the ratios of $e/H$ equal to 0.1 and 0.3 and one row of screws with the ratio of $e/H$ equal to 0.5. The screw spacings along the member length direction are shown in Figure 2. Note that all the member lengths satisfy the minimum specimen length requirement for End-Two-Flange loading tests given in AISI S909 [11]. The specimen ID starts with the nominal dimensions of the built-up I-section and followed by the ratio of $e/H$, with a symbol * referring a repeated test.

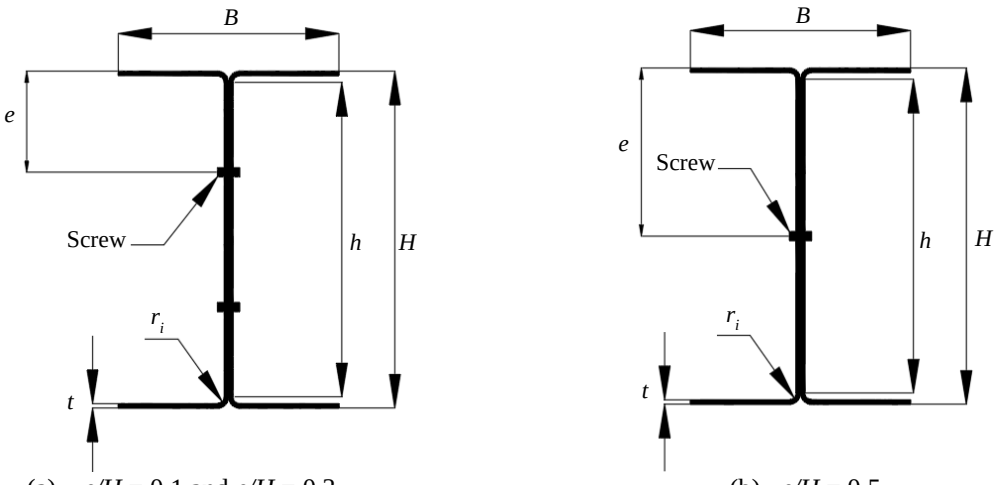


(a) $e/H$ = 0.1 and $e/H$ = 0.3 (b) $e/H$ = 0.5

Figure 1: Definitions of geometric parameters of built-up I-sections with different screw arrangements.

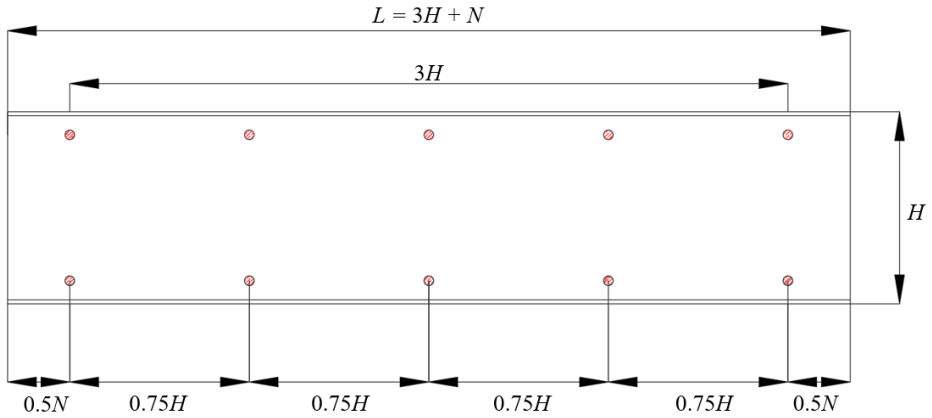


Figure 2: Definitions of geometric parameters of built-up I-sections with different screw arrangements.

Table 1: Measured geometric dimensions of austenitic and duplex stainless steel built-up I-section specimen and test failure load per web.

| Material Type | Specimen ID | $H$ (mm) | $B$ (mm) | $t$ (mm) | $r_i$ (mm) | $L$ (mm) | $N$ (mm) | $e$ (mm) | $P_t$ (kN) |
|---|---|---|---|---|---|---|---|---|---|
| Austenitic | 100 × 80 × 1.0-0.1 | 100.7 | 80.3 | 1.01 | 3.1 | 340.0 | 40 | 11.8 | 3.0 |
| | 100 × 80 × 1.0-0.3 | 101.3 | 80.1 | 0.98 | 3.1 | 340.0 | 40 | 30.6 | 2.7 |
| | 100 × 80 × 1.0-0.5 | 101.7 | 80.1 | 1.00 | 3.1 | 340.0 | 40 | 50.7 | 2.5 |
| | 125 × 90 × 1.0-0.1 | 127.0 | 90.1 | 0.98 | 3.1 | 440.0 | 65 | 13.6 | 3.1 |
| | 125 × 90 × 1.0-0.3 | 126.1 | 90.5 | 1.01 | 3.0 | 440.0 | 65 | 38.0 | 3.2 |
| | 125 × 90 × 1.0-0.5 | 126.4 | 90.2 | 1.02 | 3.3 | 440.0 | 65 | 63.1 | 2.9 |
| | 100 × 80 × 2.0-0.1 | 100.5 | 80.3 | 2.01 | 3.1 | 340.0 | 40 | 11.3 | 15.6 |
| | 100 × 80 × 2.0-0.3 | 100.4 | 80.2 | 2.04 | 3.1 | 340.0 | 40 | 31.8 | 16.2 |
| | 100 × 80 × 2.0-0.5 | 100.8 | 81.1 | 2.05 | 3.1 | 340.0 | 40 | 48.2 | 14.9 |
| | 125 × 90 × 2.0-0.1 | 125.9 | 90.6 | 2.06 | 3.3 | 440.0 | 65 | 15.0 | 19.6 |
| | 125 × 90 × 2.0-0.1* | 125.6 | 90.6 | 2.04 | 3.2 | 440.0 | 65 | 13.8 | 19.9 |
| | 125 × 90 × 2.0-0.3 | 125.8 | 90.9 | 2.01 | 3.2 | 440.0 | 65 | 39.2 | 16.6 |
| | 125 × 90 × 2.0-0.5 | 125.5 | 90.5 | 2.00 | 3.2 | 440.0 | 65 | 62.7 | 15.8 |
| | 150 × 100 × 2.0-0.1 | 150.6 | 99.5 | 2.03 | 3.1 | 515.0 | 65 | 17.0 | 14.9 |
| | 150 × 100 × 2.0-0.3 | 151.0 | 99.6 | 2.02 | 3.2 | 515.0 | 65 | 47.3 | 15.3 |
| | 150 × 100 × 2.0-0.5 | 150.4 | 99.8 | 2.03 | 3.2 | 515.0 | 65 | 74.8 | 13.3 |
| Duplex | 100 × 80 × 1.5-0.1 | 100.9 | 80.8 | 1.51 | 2.5 | 340.0 | 40 | 11.2 | 10.2 |
| | 100 × 80 × 1.5-0.3 | 100.0 | 80.6 | 1.54 | 2.5 | 340.0 | 40 | 30.9 | 12.1 |
| | 100 × 80 × 1.5-0.5 | 100.6 | 80.3 | 1.50 | 2.5 | 340.0 | 40 | 49.8 | 10.4 |
| | 125 × 90 × 1.5-0.1 | 125.3 | 91.2 | 1.52 | 2.6 | 440.0 | 65 | 12.9 | 13.0 |
| | 125 × 90 × 1.5-0.1* | 125.3 | 91.2 | 1.50 | 2.6 | 440.0 | 65 | 14.2 | 12.4 |
| | 125 × 90 × 1.5-0.3 | 125.4 | 91.2 | 1.51 | 2.6 | 440.0 | 65 | 39.0 | 11.6 |
| | 125 × 90 × 1.5-0.5 | 125.3 | 91.6 | 1.49 | 2.5 | 440.0 | 65 | 62.9 | 10.8 |

## 2.2 Material properties

Tensile coupon tests were conducted to obtain the material stress–strain curves. Flat and corner coupons were cut from representative press-braked austenitic and duplex stainless steel channel sections and employed in the material coupon tests. The geometric dimensions of all the coupons were designed to comply with the requirements in ASTM E8/E8M-22 [12]. Standard tensile coupon tests were conducted. A summary of the key measured material properties is presented in Table 2, including the Young's modulus $E$, the 0.2% proof stress $\sigma_{0.2}$, the ultimate stress $\sigma_u$, the strain at the ultimate stress $\varepsilon_u$, the fracture strain $\varepsilon_f$ and the parameters $n$ and $m$, which are used in the Ramberg-Osgood material model [13].

Table 2: Key measured material properties.

| Coupon ID | Material type | $t$ (mm) | Measured | | | | | R–O exponents | |
|---|---|---|---|---|---|---|---|---|---|
| | | | $E$ (Gpa) | $\sigma_{0.2}$ (MPa) | $\sigma_u$ (MPa) | $\varepsilon_u$ (%) | $\varepsilon_f$ (%) | $n$ | $m$ |
| Flat coupon #1 | Austenitic | 1.0 | 206.0 | 259.4 | 807.9 | 52.8 | 53.0 | 9.5 | 1.9 |
| Flat coupon #2 | Austenitic | 2.0 | 206.1 | 283.7 | 782.3 | 57.9 | 58.1 | 12.2 | 2.0 |
| Flat coupon #3 | Duplex | 1.5 | 202.1 | 568.3 | 805.8 | 24.6 | 34.1 | 7.4 | 3.0 |
| Corner coupon #1 | Austenitic | 1.0 | 189.0 | 478.6 | 933.7 | 52.1 | 54.0 | 5.5 | 2.4 |
| Corner coupon #2 | Austenitic | 2.0 | 186.4 | 488.9 | 892.9 | 46.6 | 57.1 | 13.6 | 2.5 |
| Corner coupon #3 | Duplex | 1.5 | 201.5 | 937.9 | 1114.5 | 22.7 | 28.0 | 6.9 | 3.4 |

## 2.3 Measurements of initial local geometric imperfections

The initial local geometric imperfections of each stainless steel built-up I-section specimen were measured. As shown in Figure 3, three LVDTs are placed to the mid-length and two ends of the specimen and moved transversely across the constituent plate elements of the built-up I-section. The initial local geometric imperfections for each constituent plate element were computed as the deviations from the measured data to the linear regression line fitted to the measured data, while the initial local geometric imperfection magnitude of the specimen $\omega_0$ was taken as the maximum value obtained from all the constituent plate elements, as reported in Table 3.

Table 3 Comparisons of test and numerical failure loads for measured and generalised initial local geometric imperfection magnitudes.

| Material Type | Specimen ID | $P_t/P_{FE}$ | |
|---|---|---|---|
| | | $\omega_0$ | $t$/10 |
| Austenitic | 100 × 80 × 1.0-0.1 | 1.02 | 1.00 |
| | 100 × 80 × 1.0-0.3 | 0.97 | 0.95 |
| | 100 × 80 × 1.0-0.5 | 0.99 | 0.98 |
| | 125 × 90 × 1.0-0.1 | 0.98 | 1.01 |
| | 125 × 90 × 1.0-0.3 | 0.98 | 0.98 |
| | 125 × 90 × 1.0-0.5 | 1.02 | 1.00 |
| | 100 × 80 × 2.0-0.1 | 1.01 | 1.03 |
| | 100 × 80 × 2.0-0.3 | 1.04 | 1.06 |
| | 100 × 80 × 2.0-0.5 | 1.03 | 1.05 |
| | 125 × 90 × 2.0-0.1 | 0.99 | 1.03 |
| | 125 × 90 × 2.0-0.1* | 1.03 | 1.09 |
| | 125 × 90 × 2.0-0.3 | 1.04 | 1.06 |
| | 125 × 90 × 2.0-0.5 | 1.01 | 1.06 |
| | 150 × 100 × 2.0-0.1 | 0.99 | 1.00 |
| | 150 × 100 × 2.0-0.3 | 0.98 | 0.99 |
| | 150 × 100 × 2.0-0.5 | 1.01 | 1.03 |
| Duplex | 100 × 80 × 1.5-0.1 | 1.02 | 1.02 |
| | 100 × 80 × 1.5-0.3 | 1.00 | 1.00 |
| | 100 × 80 × 1.5-0.5 | 1.05 | 1.05 |
| | 125 × 90 × 1.5-0.1 | 1.03 | 1.03 |
| | 125 × 90 × 1.5-0.1* | 1.03 | 1.03 |
| | 125 × 90 × 1.5-0.3 | 1.00 | 1.00 |
| | 125 × 90 × 1.5-0.5 | 1.03 | 1.03 |
| Mean | | 1.01 | 1.02 |
| COV | | 0.02 | 0.03 |

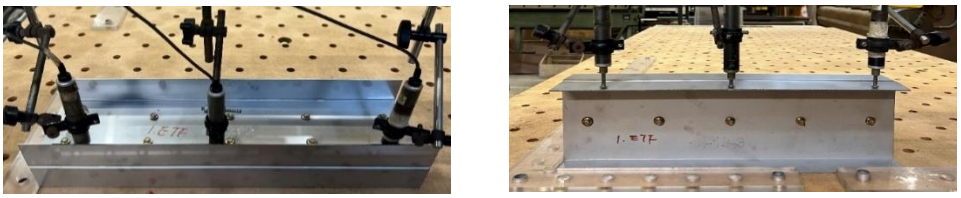

Figure 3: Test setups for initial local geometric imperfection measurements.

## 2.4 End-Two-Flange loading tests

End-Two-Flange (ETF) loading tests were conducted on a total of 23 austenitic and duplex stainless steel built-up I-section specimens. A displacement-controlled testing machine with fixed end platens was adopted to apply compression loads at a constant loading rate of 0.3 mm/min. The end of the specimen is subjected to two concentrated transverse loads applied via two identical bearing plates on both top and bottom flanges, as shown in Figure 4. The bearing plates were equipped with steel rollers to allow the in-plane rotation but without horizontal translation. Prior to testing, each specimen was carefully aligned by means of lasers and spirit levels to ensure the longitudinal centreline of the specimen was parallel to the ground level. Figure 4 depicts the instrumentation employed for the ETF loading tests, where one LVDT (LVDT 1) was vertically installed to measure the vertical deformations of the web of the built-up I-section and two LVDTs (LVDT 2 and LVDT 3) were horizontally installed to measure the lateral deformations of the web of the built-up I-section. Upon testing, all the austenitic and duplex stainless steel built-up I-section specimens failed by web crippling. A series of the failure modes of typical specimens with three screw arrangements were shown in Figure 5. The failure load per web $P_t$ is equal to half of peak load of the corresponding stainless steel built-up I-section specimen as recorded by the testing machine, and reported in Table 1.

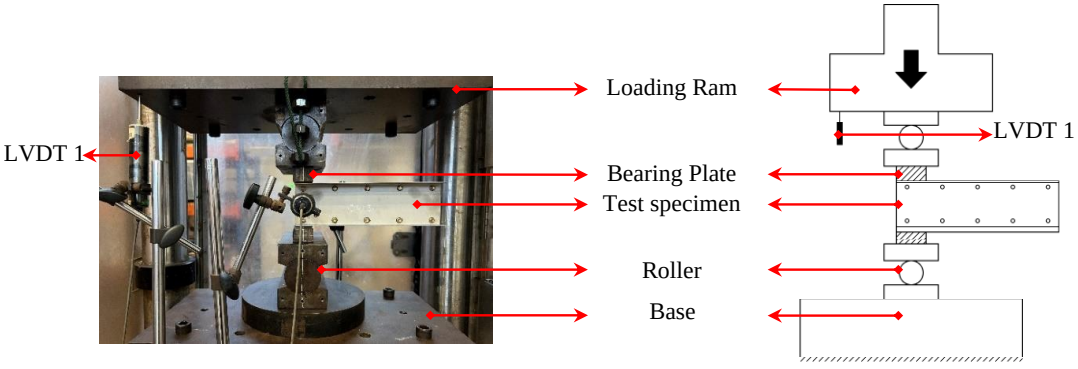


(a) Front view

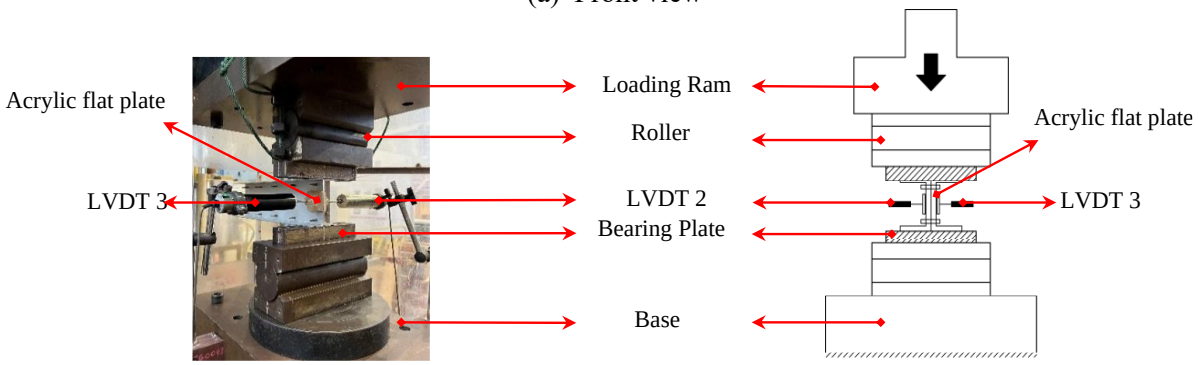


(b) Side view

Figure 4: ETF loading test setup.

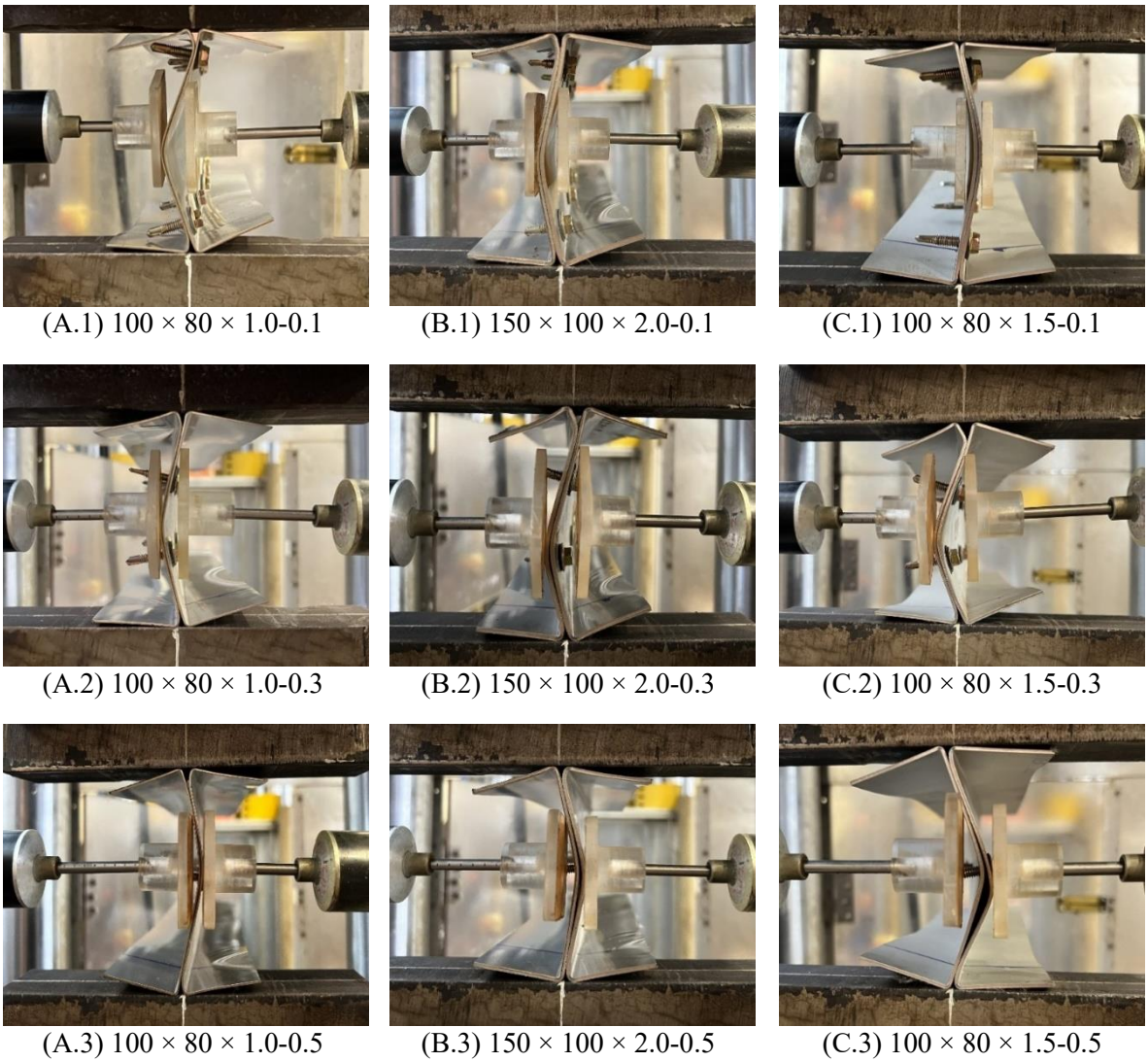

(A.1) 100 × 80 × 1.0-0.1 (B.1) 150 × 100 × 2.0-0.1 (C.1) 100 × 80 × 1.5-0.1

(A.2) 100 × 80 × 1.0-0.3 (B.2) 150 × 100 × 2.0-0.3 (C.2) 100 × 80 × 1.5-0.3

(A.3) 100 × 80 × 1.0-0.5 (B.3) 150 × 100 × 2.0-0.5 (C.3) 100 × 80 × 1.5-0.5

Figure 5: Web crippling failure modes of stainless steel built-up I-section specimens.

## 3 NUMERICAL MODELLING

### 3.1 Development of FE models

The shell element S4R [14] and the solid element C3D8R [14], which has been extensively used in previous numerical modelling of built-up section members failing by web crippling [15, 16], were employed to model the stainless steel component channel section members and self-drilling screws, respectively. Bearing plates were modelled as discrete rigid parts using the rigid element R3D4 [14]. The element size was selected to be $2.5t \times 2.5t$ for the flat portions of the channel section members. To accurately capture the curved geometries, each corner of the channel section was uniformly discretised into eight elements and a mesh with the element size of 1.5 × 1.5 × 1.5 mm was assigned to self-drilling screws. Regarding the material modelling of stainless steel, the measured engineering flat and corner stress–strain curves were firstly converted into the true stress–plastic strain curves and then incorporated into the FE models.

The ‘surface-to-surface contact’ command [14] was adopted to simulate the interaction between (i) each pair of the overlapped webs of the built-up I-section and (ii) the bearing plates and the flanges of the built-up I-section. A hard contact was adopted in the normal direction, allowing two contact faces to separate in tension but with no penetration in compression, while

a penalty method was adopted in the tangential direction, with the interaction (i) defined as frictionless and a friction coefficient of 0.45 set for the interaction (ii). The 'tie' constraint [14] was used to tie each screw and the corresponding screw holes of the channel section members, to ensure no relative motion between them. Each bearing plate was coupled to a concentric reference point. The reference point of the top bearing plate was allowed for the in-plane rotation and vertical translations, while the reference point of the bottom bearing plate was only allowed for the in-plane rotation. Initial local geometric imperfections were incorporated into the FE models by defining imperfection distribution patterns in the form of the lowest elastic local buckling mode shapes obtained from prior linear eigenvalue buckling analysis [14]. Both the measured imperfection magnitude $\omega_0$ and the generalised magnitude $t/10$ were used to factor the distribution pattern.

### 3.2 Validation

The accuracy of the developed FE models was evaluated by comparisons between the test and numerical results. Considering the measured imperfection magnitude $\omega_0$ and the generalised magnitude $t/10$, the mean test-to-numerical failure load ratios $P_t/P_{FE}$ are equal to 1.01 and 1.02, with the corresponding COVs of 0.02 and 0.03, respectively, revealing that both the measured and generalised imperfection magnitudes yielded accurate and consistent predictions of the test failure loads. The test load–lateral deformation curves were well captured by their numerical counterparts, as shown in Figure 6. Figure 7 presents the test and numerical failure modes for the stainless steel built-up I-section specimen 125 × 90 × 1.0-0.1, indicating good agreement. Overall, the experimental responses of stainless steel built-up I-section specimens can be accurately simulated by the developed FE models.

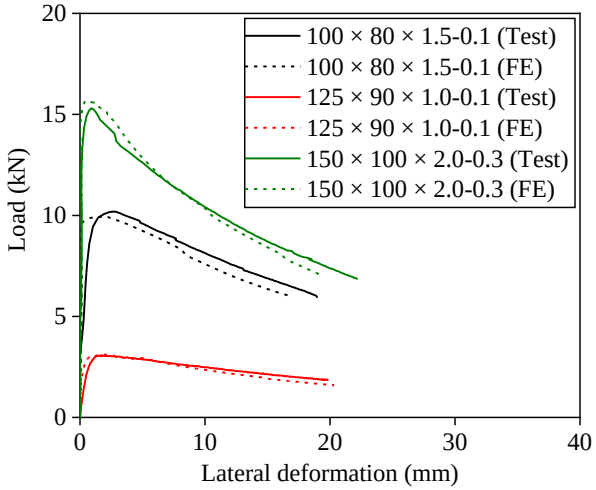


Figure 6: Comparisons of test and numerical load–lateral deformation curves for typical stainless steel built-up I-section specimens.

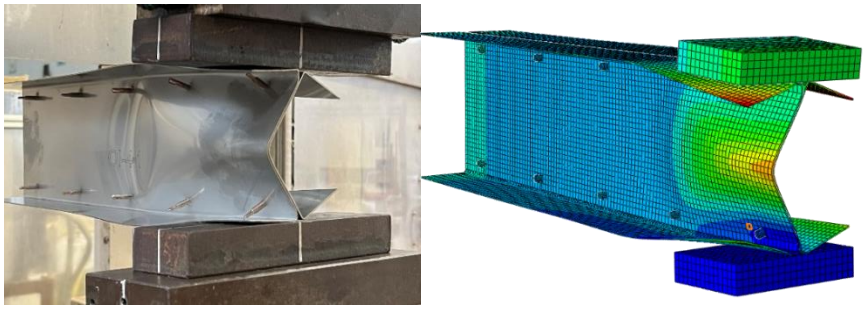

Figure 7: Test and numerical failure modes for 125 × 90 × 1.0-0.1.

### 3.3 Parametric studies

The validated FE models were employed to conduct parametric studies to generate further numerical data with various screw arrangements over a wide range of cross-section dimensions and bearing lengths. The initial local geometric imperfection magnitude was taken as *t*/10. The material properties measured from the 1.0-mm-thick and 2.0-mm-thick austenitic stainless steel plates were used for the austenitic stainless FE models with the thickness *t* smaller and larger than 2.0 mm, respectively, while the material properties measured from the 1.5-mm-thick duplex stainless steel plate were used for all the duplex stainless steel FE models. As reported in Table 4, a total of 63 austenitic and duplex stainless steel built-up I-section members were modelled. Specifically, 21 built-up I-sections, with 11 austenitic stainless steel built-up I-sections and 10 duplex stainless steel built-up I-sections, three screw arrangements, with the ratios of *e/H* equal to 0.1, 0.3 and 0.5, and different bearing lengths *N*, ranging from 80 mm to 150 mm, were considered.

Table 4 Parametric study results for stainless steel built-up I-section members.

| Material type | Built-up I-section | $r_i/t$ | $N/t$ | $P_{FE}$ (kN) | | |
|---|---|---|---|---|---|---|
| | | | | $e/H$ = 0.1 | $e/H$ = 0.3 | $e/H$ = 0.5 |
| Austenitic | 100 × 80 × 2.5 | 1.5 | 32.0 | 33.0 | 34.3 | 28.2 |
| | 100 × 80 × 3.0 | 1.1 | 26.7 | 46.2 | 48.3 | 40.9 |
| | 125 × 90 × 1.5 | 1.5 | 53.3 | 10.5 | 10.4 | 9.2 |
| | 125 × 90 × 2.5 | 0.5 | 32.0 | 31.8 | 31.9 | 29.0 |
| | 125 × 90 × 3.0 | 0.3 | 26.7 | 44.4 | 45.4 | 42.3 |
| | 150 × 100 × 1.0 | 1.5 | 90.0 | 4.0 | 4.2 | 3.5 |
| | 150 × 100 × 1.5 | 0.7 | 60.0 | 10.8 | 11.3 | 9.5 |
| | 200 × 120 × 1.5 | 1.5 | 66.7 | 8.9 | 9.3 | 7.6 |
| | 200 × 120 × 2.0 | 0.9 | 50.0 | 17.5 | 17.5 | 14.9 |
| | 350 × 200 × 2.0 | 1.9 | 75.0 | 13.8 | 14.5 | 13.1 |
| | 350 × 200 × 2.5 | 1.3 | 60.0 | 23.3 | 24.2 | 21.6 |
| Duplex | 100 × 80 × 2.0 | 2.1 | 40.0 | 30.3 | 32.4 | 26.8 |
| | 100 × 80 × 3.0 | 1.1 | 26.7 | 75.4 | 80.1 | 68.2 |
| | 100 × 80 × 2.5 | 1.5 | 32.0 | 50.8 | 54.0 | 45.4 |
| | 125 × 90 × 2.0 | 0.9 | 40.0 | 29.5 | 29.2 | 25.2 |
| | 125 × 90 × 3.0 | 0.3 | 26.7 | 75.2 | 72.9 | 64.5 |
| | 150 × 100 × 1.5 | 0.7 | 60.0 | 12.7 | 13.9 | 10.8 |
| | 150 × 100 × 2.5 | 0.2 | 36.0 | 47.8 | 48.8 | 37.6 |
| | 200 × 120 × 1.5 | 1.5 | 66.7 | 9.5 | 10.7 | 8.3 |
| | 200 × 120 × 2.0 | 0.9 | 50.0 | 20.3 | 22.0 | 17.7 |
| | 350 × 200 × 3.0 | 0.9 | 50.0 | 40.4 | 41.6 | 35.3 |

## 4 DESIGN

### 4.1 European code EN 1993-1-4 (EC3)

For the design of stainless steel built-up I-section members under ETF loading failing by web crippling, EN 1993-1-4 [9] adopts the same design rules as those specified in EN 1993-1-3 [17] for carbon steel built-up I-section members. The EC3 design failure load per web is given by Eq. (1), where *k* is a material factor and equal to $\sigma_{0.2}$ / 228 and $h_w$ is the distance between centrelines of two flanges.

$$P_{u,EC3} = \frac{1}{k}(0.98 - \frac{h_w}{865t})(0.64 + \frac{0.31t}{1.9})(8.8 + 1.1\sqrt{\frac{N}{t}})t^2\sigma_{0.2} \quad (1)$$

The EC3 failure load predictions for austenitic and duplex stainless steel built-up section members were assessed by comparing against the test and numerical failure loads per web. As

reported in Table 5, the mean test and numerical to EC3 predicted failure load ratios $P_u/P_{u,EC3}$ are equal to 1.33 and 1.94, with the corresponding COVs of 0.14 and 0.21, for austenitic and duplex stainless steel built-up I-section members, respectively. The graphical assessment results are shown in Figure 8, where the test and numerical to EC3 predicted failure load ratios $P_u/P_{u,EC3}$ are plotted against the web flat width to thickness ratios $h/t$. It can be concluded that (i) EN 1993-1-4 [9] resulted in overly conservative and scattered failure load predictions and (ii) the level of inaccuracy and inconsistency is higher for built-up I-section members made of duplex stainless steel.

Table 5 Comparisons of test and numerical failure loads with predicted failure loads.

| Material type | No. of test data | No. of FE data | EN 1993-1-4 | | ASCE/SEI 8-22 | | Proposed | |
|---|---|---|---|---|---|---|---|---|
| | | | Mean | COV | Mean | COV | Mean | COV |
| Austenitic | 16 | 33 | 1.33 | 0.14 | 1.08 | 0.11 | 1.15 | 0.07 |
| Duplex | 7 | 30 | 1.94 | 0.21 | 0.77 | 0.19 | 1.15 | 0.09 |
| Total | 23 | 63 | 1.60 | 0.27 | 0.95 | 0.21 | 1.15 | 0.08 |

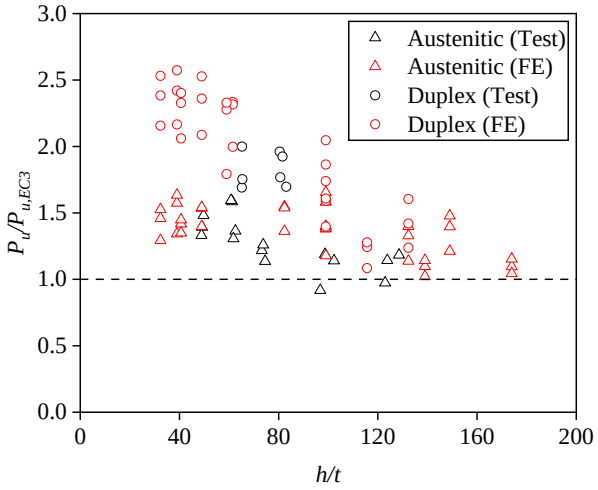


Figure 8: Comparison of test and numerical failure loads with predicted failure loads from EN 1993-1-4.

## 4.2 American specification ASCE/SEI 8-22 (ASCE)

The ASCE/SEI 8-22 [10] specifies that the web crippling resistances per web $P_{u,ASCE}$ for stainless steel built-up I-section members under ETF loading is determined by Eq. (2), where the angle between the plane of web and the plane of bearing surface $\theta$ is equal to 90° and the coefficients, including the general coefficient $C$, the inner radius coefficient $C_R$, the bearing length coefficient $C_N$ and the web slenderness coefficient $C_h$, are taken equal to 15.5, 0.09, 0.08 and 0.04 for stainless steel built-up I-section members, respectively. The values of coefficients vary depending on the support and flange conditions, load cases as well as the types of cross-sections.

$$P_{u,ASCE} = C \sin\theta (1 - C_R \sqrt{\frac{r_i}{t}})(1 + C_N \sqrt{\frac{N}{t}})(1 - C_h \sqrt{\frac{h}{t}}) t^2 \sigma_{0.2} \tag{2}$$

The ASCE design rules were assessed by comparing the predicted failure loads against the test and numerical failure loads. As reported in Tables 5, the ASCE design rules were shown to yield inaccurate and scattered failure load predictions, with the mean ratios of $P_u/P_{u,ASCE}$ equal to 1.08 and 0.77 and the corresponding COVs of 0.11 and 0.19 for built-up I-section members made of austenitic and duplex stainless steel, respectively. Many of the ASCE design failure

loads are unsafe, especially for duplex stainless steel built-up I-section members, as reflected by the data points lying below the reference line in Figure 9.

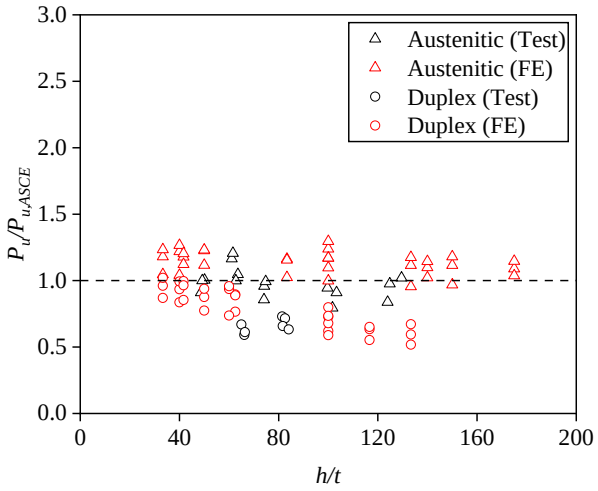


Figure 9: Comparison of test and numerical failure loads with predicted failure loads from ASCE/SEI 8-22.

### 4.3 Improved design approach

Addressing the shortcomings of the existing design rules, a new design approach was proposed for predicting failure loads of austenitic and duplex stainless steel built-up I-section members failing by web crippling. The new design expression, as given by Eq. (3), followed the general format of the ASCE design expression, but with a new coefficient $C_e$ to consider the effect of screw arrangements and modified values of coefficients $C$, $C_R$, $C_N$ and $C_h$ derived by means of least squares regression analyses and reported in Table 6. The quantitative assessment results are shown in Table 5, where the mean ratios of $P_u/P_{u,pr}$ are equal to 1.15, with the corresponding COVs of 0.07 and 0.09 for austenitic and duplex stainless steel built-up I-section members, respectively. The graphical assessment results are shown in Figure 10, revealing that the proposed design approach led to accurate, consistent and conservative failure load predictions for austenitic and duplex stainless steel built-up I-section members.

$$P_{u,pr} = C \sin\theta (1 - C_R \sqrt{\frac{r_i}{t}})(1 + C_N \sqrt{\frac{N}{t}})(1 - C_h \sqrt{\frac{h}{t}})(1 - C_e \sqrt{\frac{e}{h}}) t^2 \sigma_{0.2} \quad (3)$$

Table 6 Proposed coefficients for new design approach.

| Material type | $C$ | $C_R$ | $C_N$ | $C_h$ | $C_e$ |
|---|---|---|---|---|---|
| Austenitic | 10.7 | 0.28 | 0.45 | 0.05 | 0.26 |
| Duplex | 29.4 | 0.63 | 0.48 | 0.07 | 0.28 |

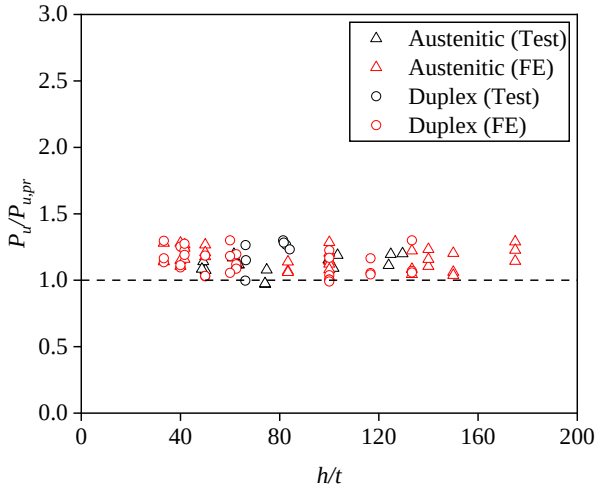


Figure 10: Comparison of test and numerical failure loads with predicted failure loads from proposed design approach.

## 5 CONCLUSIONS

The web crippling behaviour and resistances of austenitic and duplex stainless steel built-up I-section members have been investigated through testing and numerical modelling. The experimental programme included under ETF loading tests on a total of 23 austenitic and duplex stainless steel built-up I-section specimens. The observed test results were fully reported and discussed. Subsequently, a numerical modelling programme was carried out and included the development and validation of FE models and a series of parametric studies to generate further numerical data. On the basis of the obtained experimental and numerical data, the accuracy of the existing codified design rules for stainless steel built-up I-section members, as prescribed in EN 1993-1-4 [9] and ASCE/SEI 8-22 [10], was evaluated. The evaluation results revealed that EN1993-1-4 [9] yielded overly conservative and scattered failure load predictions, while the ASCE/SEI 8-22 [10] led to unconservative and scattered predictions of failure load. An improved design approach was then proposed and shown to result in a higher level of design accuracy, consistency and safety over the existing design codes.

## REFERENCES

[1] Gardner L. “Stability and design of stainless steel structures–Review and outlook”. *Thin-Walled Structures*, **141**, 208–16, 2019.

[2] Baddoo NR. “Stainless steel in construction: A review of research, applications, challenges and opportunities”. *Journal of Constructional Steel Research*, **64**, 1199–206, 2008.

[3] Yousefi AM, Lim JBP, Clifton GC. “Web crippling design of cold-formed ferritic stainless steel unlipped channels with fastened flanges under end-two-flange loading condition”. *Journal of Constructional Steel Research*, **152**, 12–28, 2019.

[4] Yousefi AM, Lim JBP, Clifton GC. “Web crippling strength of perforated cold-formed ferritic stainless steel unlipped channels with restrained flanges under one-flange loadings”. *Thin-Walled Structures*, **137**, 94–105, 2019.

[5] Zhou F, Young B. “Experimental and numerical investigations of cold-formed stainless steel tubular sections subjected to concentrated bearing load”. *Journal of Constructional Steel Research*; **63**, 1452–66, 2007.

[6] Zhou F, Young B. “Web crippling of cold-formed stainless steel tubular sections”. *Advances in Structural Engineering*, **11**, 679–91, 2008.

[7] Cai Y, Young B. “Web crippling of lean duplex stainless steel tubular sections under concentrated end bearing loads”, *Thin-Walled Structures*, **134**, 29–39, 2019.

[8] Li H-T, Young B. “Web crippling of cold-formed ferritic stainless steel square and rectangular hollow sections”, *Engineering Structures*, **176**, 968–80, 2018.

[9] European Committee for Standardization (EC3). Eurocode 3: design of steel structures - part 1-4: General rules - Supplementary rules for stainless steels. EN1993-1-4. Brussels, Belgium: European committee for standardization (CEN); 2023.

[10] American Society of Civil Engineers. Specification for the Design of Cold-Formed Stainless Steel Structural Members, ASCE-8-22. Reston, Virginia: American Society of Civil Engineers; 2022.

[11] American Iron and Steel Institute (AISI). Test Standard for Determining the Web Crippling Strength of Cold Formed Steel Flexural Members, 2017 Edition. AISI S909-17. Washington DC, USA: AISI; 2018.

[12] American Society for Testing and Materials (ASTM). Standard Test Methods for Tension Testing of Metallic Materials. E8/E8M-22. West Conshohocken, PA., USA: ASTM International; 2022.

[13] Arrayago I, Real E, Gardner L. “Description of stress–strain curves for stainless steel alloys”. *Materials & Design*, **87**, 540–52, 2015.

[14] ABAQUS. ABAQUS Analysis User’s Manual, Version 6.17. Dassault Systems Simulia Corp, Providence, RI, USA; 2017.

[15] He J, Young B. “Web crippling design of cold-formed steel built-up I-sections”. *Engineering Structures*, **252**,113731, 2022.

[16] He J, Young B. “Web crippling of cold-formed steel built-up box sections”. *Thin-Walled Structures*, **171**, 108789, 2022.

[17] European Committee for Standardization (EC3). Eurocode 3: design of steel structures - part 1-3: general rules-supplementary rules for cold-formed members and sheeting. EN1993-1-3. Brussels, Belgium: European committee for standardization (CEN); 2006.